Inorg. Chem. **2006**, *45*, 3864–3877

Thallophilic Interactions in Aryloxide Compounds: the $\{Tl_2(\mu_2\text{-}OAr)_4\}$ Structural Motif in $(TlOAr)_4$ and $Tl_2Cu(OAr)_4$ Compounds

Montana V. Childress,[†] David Millar,[†] Todd M. Alam,[‡] Kevin A. Kreisel,[§] Glenn P. A. Yap,[§] Lev N. Zakharov,[£] James A. Golen,[£,#] Arnold L. Rheingold,[£] and Linda H. Doerrer*,[†]

Chemistry Department, Barnard College, 3009 Broadway, New York, New York 10027, Department of Chemical Analysis and Remote Sensing, Sandia National Laboratories, MS 0886, Albuquerque, New Mexico 87185-0886, Department of Chemistry and Biochemistry, University of Delaware, Newark, Delaware 19716, Department of Chemistry and Biochemistry, University of California, San Diego, 9500 Gilman Drive, La Jolla, California 92093-0358, and Department of Chemistry and Biochemistry, University of Massachusetts, Dartmouth, North Dartmouth, Massachusetts 02747

Received June 13, 2005

Two thallium aryloxide compounds $TlOC_6F_5$ ($TlOAr^F$) and bis-3,5-$TlOC_6H_3(CF_3)_2$ ($TlOAr'$) have been recrystallized from THF and crystallographically characterized in different isomeric forms. The latter compound forms a solvated tetrameric cubane, $\{TlOAr'\}_4$·THF, **1**. The $TlOAr^F$ compound crystallized with a similar stoichiometry, $\{TlOAr^F\}_4$·2 THF, **2**, but contains a $\{Tl_2(\mu_2\text{-}OAr^F)_4\}$ unit that includes a thallophilic interaction at a distance of 3.5943(15) Å. Solution ^{205}Tl and ^{203}Tl NMR studies of **1** and **2** support the retention of a cubane structure for **1** in solution and suggest a similar structure for **2** with coupled thallium centers down to –90 °C. Fluorescence spectroscopy data for both compounds **1** and **2** in THF are consistent with LMCT. DFT calculations of **1**, **2**, and three models of the $\{Tl_2(\mu_2\text{-}OAr^F)_4\}$ unit show a bonding overlap of the bridged thallium atoms in **2** and are also used to describe the bonding in **1**. The structures of two heterobimetallic compounds, $Tl_2Cu(OAr^F)_4$, **4,** and $Tl_2Cu(OAr')_4$, **5**, with the $\{Tl_2(\mu_2\text{-}OAr^F)_4\}$ structural motif and thallophilic contacts of 3.86(6) and 3.564(1) Å, respectively, are described. The crystal structures of the unsolvated of $TlOAr^F$, **2b**, solvated heterobimetallic derivative $Tl_2Cu(OAr')_4$·2THF, **5b**, and the monomeric (18-crown-6)$TlOAr^F$, **3**, and ^{205}Tl NMR spectra of $TlOC_6H_5$, **6**, are also reported for comparison purposes.

Introduction

Metallophilicity is increasingly acknowledged as a measurable and demonstrable force in chemical bonding.[1] Metallophilicity is the affinity of two metals with closed subshell electron configurations for one another, such as d^{10} (Au^+, Ag^+, Cu^+, Pt^0) or $d^{10}s^2$ (Tl^+, Hg^0). The term "aurophilic" was first coined by Schmidbaur on the basis of numerous examples in gold chemistry.[2] Both homo- and heterobimetallic systems have been investigated since, including the more specific terms of aurophilicity, argentophilicity, and cuprophilicity being used for homometallic gold, silver, and copper examples. Current theoretical understanding[3] describes metallophilicity as a type of dispersion or electron correlation interaction in which both ionic terms[4] and relativistic effects play a role for 5d and 6p elements.

* To whom correspondence should be addressed. E-mail: ldoerrer@barnard.edu.
[†] Barnard College.
[‡] Sandia National Laboratories.
[§] University of Delaware.
[£] University of California, San Diego.
[#] University of Massachusetts, Dartmouth.

(1) Pyykkö, P. *Chem. Rev.* **1997**, *97*, 597−636.
(2) Schmidbaur, H. *Gold Bull.* **2000**, *33*, 3−10.
(3) Pyykkö, P.; Runeberg, N.; Mendizabal, F. *Chem. Eur. J.* **1997**, *3*, 1451−1457.
(4) Runeberg, N.; Schutz, M.; Werner, H.-J. *J. Chem. Phys.* **1999**, *110*, 7210−7215.
(5) Bondi, A. *J. Phys. Chem.* **1964**, *68*, 441−451.
(6) Ford, P. C.; Vogler, A. *Acc. Chem. Res.* **1993**, *26*, 220−6.
(7) Fernandez, E. J.; Laguna, A.; Lopez-de-Luzuriaga, J. M.; Monge, M.; Montiel, M.; Olmos, M. E.; Perez, J. *Organometallics* **2004**, *23*, 774−782.
(8) Fernandez, E. J.; Laguna, A.; Lopez-De-Luzuriaga, J. M.; Mendizabal, F.; Monge, M.; Olmos, M. E.; Perez, J. *Chem. Eur. J.* **2003**, *9*, 456−465.
(9) Maroni, V. A.; Spiro, T. G. *Inorg. Chem.* **1968**, *7*, 193−7.
(10) Quicksall, C. O.; Spiro, T. G. *Inorg. Chem.* **1970**, *9*, 1045−9.

10.1021/ic050955o CCC: $33.50
Published on Web 01/26/2006

Experimental demonstrations of metallophilic interactions are primarily structural ones. If two metals are closer than the sum of two van der Waals radii (3.92 Å for Tl),[5] a metallophilic interaction is inferred. Fluorescence spectroscopy studies in the solid state and solution demonstrate ligand-to-metal charge transfer (LMCT) population of metal-based orbitals[6−8] via significant Stokes shifts. Raman data have also demonstrated metal−metal interactions with thallium[9] and lead.[10]

Thallium−thallium interactions (considered here as less than 4.0 Å contact between thallium atoms) have been observed previously in a variety of systems[11] and structurally characterized in many cases.[12] The shortest Tl···Tl contacts (ca. 2.9 Å) occur between two covalently bonded Tl(II) centers[13−15] or between Tl(II) centers in mixed-valent Tl(I)-Tl(II) systems.[16,17] Bonding between thallium atoms has also been observed in thallium(I) amide compounds,[18,19] pyrazolyl borate derivatives,[20−25] and several in thallium(I) organometallic species.[26−30] There is also a handful of examples with bonding in bimetallic[31] or cluster compounds,[32] as well as with sulfur[33,34] or phosphorus donor atoms.[35] Thallophillic interactions (as distinct from thallophilic organisms[36]) have been explicitly named only recently.[37]

Bonding between thallium atoms in compounds with oxygen atom donor ligands has been much less frequently observed and only recently reviewed.[11] Thallium compounds with oxygen donors and Tl···Tl contacts of less than 4 Å have been observed in Tl(III) systems,[38,39] carboxylates,[37,40] acetylacetonates,[7,41] a few aryloxide systems,[42,43] and a small group of other ligands.[44−49] We have discovered a new structural motif for thallium aryloxides with a prominent thallophilic interaction and herein report its structural and spectroscopic characterization in three new compounds and a theoretical description of the electronic structure.

Experimental Section

The syntheses and some spectroscopic characterization of $TlOAr^F$, TlOAr′, $[Tl_2Cu(OAr^F)_4]$, and $[Tl_2Cu(OAr')_4]$ have been previously reported by us.[50] Elemental analyses: **1**·THF Anal. Calcd. for $C_{36}H_{20}O_5F_{24}Tl_4$: C, 23.94; H, 1.12; F, 25.24. Found: C, 24.08; H, 1.10; F 25.17. **2** Anal. Calcd. for $C_{24}O_4F_{20}Tl_4$: C, 18.60; F, 24.52. Found: C, 18.56; F, 25.32. NMR spectra were obtained on a Bruker DRX400 instrument at 230.9 and 228.8 MHz for ^{205}Tl and ^{203}Tl, respectively. All spectra were obtained using a $\pi/4$ pulse of 4.5 μs using a 1 s recycle delay on a specially tuned Tl{^{1}H} 5 mm probe using WALTZ16 ^{1}H decoupling. No ^{19}F decoupling was employed. Spectra were externally referenced to 0.001 M $Tl(NO_3)$ in D_2O (δ = 0.0 ppm) at 25 °C. Spectra simulations were obtained using the software program DMFIT.[51] Fluorescence spectra were collected on an SPEX Industries, Fluorolog-2 spectrometer with Datamax V.2.01 software with 0.1 mM solutions of **1** and **2** in THF.

A summary of crystal data collection and refinement parameters is presented in Table 1. Data were collected either on a Bruker P4/CCD or Bruker SMART APEX CCD diffractometer using graphite-monochromated Mo Kα radiation (λ = 0.71073 Å) at room (**3**), and low temperature (213 (**1**, **2b**), 200 (**2**), 218 (**4**, **5b**), and 100 K (**5**)). All data sets were corrected for absorption using SADABS multiscan method.[52] Space groups were determined on the basis of systematic absences (**3**, **5**, **5b**), intensities statistics (**2b**,

(11) Dias, H. V. R. *Compr. Coord. Chem. II* **2004**, *3*, 445−447.
(12) Allen, F. H. *Acta Crystallogr.* **2002**, *B58*, 380−388 (including February 2005 update).
(13) Henkel, S.; Klinkhammer, K. W.; Schwarz, W. *Angew. Chem., Int. Ed. Engl.* **1994**, *33*, 681−683.
(14) Wiberg, N.; Blank, T.; Amelunxen, K.; Noth, H.; Schnockel, H.; Baum, E.; Purath, A.; Fenske, D. *Eur. J. Inorg. Chem.* **2002**, 341−350.
(15) Wiberg, N.; Amelunxen, K.; Blank, T.; Lerner, H.-W.; Polborn, K.; Noeth, H.; Littger, R.; Rackl, M.; Schmidt-Amelunxen, M.; Schwenk-Kircher, H.; Warchold, M. *Z. Naturforsch. B., Chem. Sci.* **2001**, *56*, 634−651.
(16) Wiberg, N.; Blank, T.; Lerner, H.-W.; Fenske, D.; Linti, G. *Angew. Chem., Int. Ed.* **2001**, *40*, 1232−1235.
(17) Hellmann, K. W.; Gade, L. H.; Steiner, A.; Stalke, D.; Moeller, F. *Angew. Chem., Int. Ed. Engl.* **1997**, *36*, 160−163.
(18) Gade, L. H. *Dalton Trans.* **2003**, 267−278.
(19) Gade, L. H. *Angew. Chem., Int. Ed.* **2001**, *40*, 3573−3575.
(20) Janiak, C. *Main Group Met. Chem.* **1998**, *21*, 33−49.
(21) Ciunik, Z.; Ruman, T.; Lukasiewicz, M.; Wolowiec, S. *J. Mol. Struct.* **2004**, *690*, 175−180.
(22) Rheingold, A. L.; Liable-Sands, L. M.; Trofimenko, S. *Chem. Commun.* **1997**, 1691−1692.
(23) Rheingold, A. L.; Haggerty, B. S.; Liable-Sands, L. M.; Trofimenko, S. *Inorg. Chem.* **1999**, *38*, 6306−6308.
(24) Ferguson, G.; Jennings, M. C.; Lalor, F. J.; Shanahan, C. *Acta Crystallogr.* **1991**, *C47*, 2079−82.
(25) Ghosh, P.; Rheingold, A. L.; Parkin, G. *Inorg. Chem.* **1999**, *38*, 5464−5467.
(26) Janiak, C. *Coord. Chem. Rev.* **1997**, *163*, 107−216.
(27) Wright, R. J.; Phillips, A. D.; Hino, S.; Power, P. P. *J. Am. Chem. Soc.* **2005**, *127*, 4794−4799.
(28) Schebaum, L. O.; Jutzi, P. *ACS Symp. Ser.* **2002**, *822*, 16−30.
(29) Uhl, W. *Adv. Organomet. Chem.* **2004**, *51*, 53−108.
(30) Power, P. P. *J. Chem. Soc., Dalton Trans.* **1998**, 2939−2951.
(31) Fernandez, E. J.; Lopez-de-Luzuriaga, J. M.; Monge, M.; Olmos, M. E.; Perez, J.; Laguna, A. *J. Am. Chem. Soc.* **2002**, *124*, 5942−5943.
(32) Schollenberger, M.; Nuber, B.; Ziegler, M. L.; Hey-Hawkins, E. *J. Organomet. Chem.* **1993**, *460*, 55−66.
(33) Krebs, B.; Broemmelhaus, A. *Z. Anorg. Allg. Chem.* **1991**, *595*, 167−82.
(34) Krebs, B.; Broemmelhaus, A.; Kersting, B.; Nienhaus, M. *Eur. J. Solid State Inorg. Chem.* **1992**, *29*, 167−80.
(35) Shapiro, I. R.; Jenkins, D. M.; Thomas, J. C.; Day, M. W.; Peters, J. C. *Chem. Commun.* **2001**, 2152−2153.
(36) Hoffmann, G.; Schweiger, P.; Scholl, W. *Landwirt. Forsch.* **1982**, *35*, 45−54.
(37) Wiesbrock, F.; Schmidbaur, H. *J. Am. Chem. Soc.* **2003**, *125*, 3622−3630.
(38) Milburn, G. H. W.; Truter, M. R. *J. Chem. Soc. A* **1967**, 648−51.
(39) Luth, H.; Truter, M. R. *J. Chem. Soc. A* **1970**, 1287−3.
(40) Oddon, Y.; Tranquard, A.; Mentzen, B. F. *Inorg. Chim. Acta* **1981**, *48*, 129−32.
(41) Atencio, R.; Barbera, J.; Cativiela, C.; Lahoz, F. J.; Serrano, J. L.; Zurbano, M. M. *J. Am. Chem.* Soc. **1994**, *116*, 11558−11559.
(42) Harrowfield, J. M.; Sharma, R. P.; Skelton, B. W.; White, A. H. *Aust. J. Chem.* **1998**, *51*, 735−745.
(43) Mahjoub, A. R.; Morsali, A.; Bagherzadeh, H. *Polyhedron* **2002**, *21*, 2555−2560.
(44) Keefer, L. K.; Wang, S. M.; Anjo, T.; Fanning, J. C.; Day, C. S. *J. Am. Chem. Soc.* **1988**, *110*, 2800−6.
(45) Valderrama, M.; Scotti, M.; Campos, P.; Werner, H.; Mueller, G. *Chem. Ber.* **1990**, *123*, 1005−11.
(46) Playa, N.; Macias, A.; Varela, J. M.; Sanchez, A.; Casas, J. S.; Sordo, J. *Polyhedron* **1991**, *10*, 1465−72.
(47) Deacon, G. B.; Delbridge, E. E.; Forsyth, C. M.; Skelton, B. W.; White, A. H. *Dalton Trans.* **2000**, 745−751.
(48) Skopenko, V. V.; Ponomareva, V. V.; Simonov, Y. A.; Domasevich, K. V.; Dvorkin, A. A. *Zh. Neorg. Khim.* **1994**, *39*, 1332−9.
(49) Domasevich, K. V.; Skopenko, V. V.; Mokhir, A. A. *Zh. Neorg. Khim.* **1995**, *40*, 781−6.
(50) Buzzeo, M. C.; Iqbal, A. H.; Long, C. M.; Millar, D.; Patel, S.; Pellow, M. A.; Saddoughi, S. A.; Smenton, A. L.; Turner, J. F. C.; Wadhawan, J. D.; Compton, R. G.; Golen, J. A.; Rheingold, A. L.; Doerrer, L. H. *Inorg. Chem.* **2004**, *43*, 7709−7725.
(51) Massiot, D.; Fayon, F.; Capron, M.; King, I.; Le Calvé, S.; Alonso, B.; Durand, J.-O.; Bujoli, B.; Gan, Z.; Hoatson, G. *Magn. Reson. Chem.* **2002**, *40*, 70−76.
(52) Sheldrick, G. M. *SADABS: Area Detector Absorption Correction*, University of Göttingen: Göttingen, Germany, 2001.

Table 1. Summary of X-ray Crystallographic Parameters

	1	2	2b	3	4	5	5b
formula	$C_{36}H_{20}F_{24}O_5Tl_4$	$C_{16}H_8F_{10}O_3Tl_2$	C_6F_5OTl	$C_{18}H_{24}F_5O_7Tl_1$	$C_{152}H_{40}Cu_5F_{100}O_{22}Tl_{10}$	$C_{34}H_{14}CuF_{24}O_{4.50}Tl_2$	$C_{20}H_{14}Cu_{0.5}F_{12}O_3Tl$
fw	1806.01	836.6	387.43	651.74	6479.24	1422.73	766.45
cryst syst	monoclinic	monoclinic	triclinic	monoclinic	triclinic	orthorhombic	orthorhombic
space group	*C*2/*c*	*C*2/*m*	$P\bar{1}$	$P2_1/n$	$P\bar{1}$	*Pbcn*	*Pbcn*
a, Å	22.3790(16)	14.288(5)	4.1823(7)	11.0323(10)	14.8580(8)	15.3095(8)	15.627(3)
b, Å	20.8008(15)	19.253(7)	9.2088(15)	8.5110(10)	20.1452(11)	30.0215(17)	18.813(3)
c, Å	9.7563(7)	7.439(3)	9.7104(16)	23.6162(10)	28.5113(16)	16.7395(9)	15.799(3)
α, deg	–	–	107.052(3)	- -	96.734(1)	–	–
β, deg	92.8680(10)	114.124(4)	101.884(3)	100.102(10)	94.611(1)	–	–
γ, deg	–	–	90.844(3)	–	93.648(1)	–	–
V, Å^3	4535.9(6)	1867.8(12)	348.75(10)	2183.1(3)	8424.6(8)	7693.7(7)	4644.7(13)
Z, *Z*′	4, 0.5	4, 0.5	2, 1	4, 1	2, 1	8, 1	8,1
ρ(calcd), g cm^{-3}	2.645	3.012	3.689	1.983	2.554	2.457	2.192
μ(Mo Kα), mm^{-1}	14.306	17.347	23.202	7.477	10.317	9.063	7.517
T, K	213(2)	200(2)	213(2)	293	218(2)	100(2)	218(2)
R(*F*), %[a]	4.56	3.42	3.10	3.25	6.58	4.64	5.68
R(*wF*^{2}),%[b]	11.50	7.88	7.89	3.90	14.86	9.67	12.47

[a] $R = \sum||F_o| - |F_c||/\sum|F_o|$. [b] $R(\omega F^2) = \{\sum[\omega(F_o^2 - F_c^2)^2]/\sum[\omega(F_o^2)^2]\}^{1/2}$; $\omega = 1/[\sigma^2(F_o^2) + (aP)^2 + bP]$, $P = [2F_c^2 + \max(F_o,0)]/3$.

4), or systematic absences and intensities statistics (**1**, **2**). Structures were solved using direct methods and refined with full-matrix least-squares methods based on F^2. Several structures display co-crystallized solvent molecules: one THF molecule in **1** and **2**, two THF and four benzene molecules in **4**, 0.5 THF molecules per asymmetric unit in **5**, and one THF in **5b**. The THF molecule in **5** is disordered over two positions (in a 1:1 ratio), giving rise to two possible opposite orientations of the THF molecules and therefore two different positions of the THF molecules relative to the different Tl(1) atoms. The THF molecule in **1** and some CF_3 groups in **5** and **5b** are disordered over two positions. All non-H atoms were refined with anisotropic thermal parameters except solvent benzene molecules in **4**, which were refined with isotropic thermal parameters. All hydrogen atoms were treated as idealized contributions. All structure factors and anomalous displacement parameters are included in various versions of the SHELXTL program library.[53]

DFT calculations used a QS8-2400C computer from Parallel Quantum Solutions (PQS) with the Amsterdam Density Functional Package 2004.01[54−56] on all electron, geometry optimized systems with TZ2P basis sets, the Vosko, Wilk, and Nusair[57] local density approximation, and scalar relativistic corrections. Calculations were carried out on eight species: **1**, cubane $(TlOAr')_4{\cdot}2THF$ (**1b**), **2**, and the hypothetical dimers $(TlOAr')_2$, **I**, and $(TlOAr^F)_2$, **II**. Calculations carried out on models $[Tl_2(\mu_2\text{-}O)_4]^{6-}$, **2a**, $[Tl_2(\mu_2\text{-}OH)_4]^{2-}$, **2b**, and $[Tl_2(\mu_2\text{-}OAr^F)_4]^{2-}$, **2c**, used frozen 1s (large) cores on oxygen atoms, frozen 5s, 5p, 5d, and 4f (large) cores on thallium atoms, single-point systems with DZP basis sets, the Vosko, Wilk, and Nusair[57] local density approximation, and no relativistic corrections.

Results and Discussion

Structural Characterization. Previously observed structural motifs in thallium aryloxides include the cubane,[42] a dimer,[58,59] and infinite chains.[60] Factors determining the aryloxide structures include steric bulk of the ortho substituents, solubility, and relative basicity of the phenoxides. Our research has made extensive use of two fluorinated aryloxide compounds, $TlOC_6F_5$ ($TlOAr^F$) and $TlOC_6H_3(CF_3)_2$-($TlOAr'$),[50,61] that are similar in their electronic, solubility, and steric (ortho positions) properties. Remarkably, these two compounds crystallize from the same solvent in different structures, one of which is a new $\{TlOAr\}_4$ motif. This motif has been observed also in two heterobimetallic compounds, **4** and **5**, from our laboratory as described below. X-ray crystallographic data collection parameters for all compounds are given in Table 1. Selected distances and angles for (TlOAr) compounds are given in Table 2 and those for $[Tl_2$-$Cu(OAr)_4]$ compounds in Table 3.

The structure of **1**, shown in Figure 1, is a slightly distorted cubane composed of four $TlOAr'$ units that form two interpenetrating tetrahedra, one of thallium and one of oxygen atoms. Such structures also have been seen previously in thallium alkoxides.[60] One molecule of THF in **1** is bonded to Tl(2) with a Tl(2)···O(1S) distance of 2.5569 Å. The carbon positions of the THF molecule are disordered over two positions. The angles at each oxygen corner are noticeably obtuse ($Tl-O-Tl_{avg} = 101(4)°$) and those at thallium necessarily acute ($O-Tl-O_{avg} = 77(2)°$) compared to a perfect cube, consistent with other thallium cubane structures.[42,60,62] The thallium−thallium distances of $Tl-Tl_{avg} = 4.02(11)$ Å in **1** are too long for strong bonding interactions.

Thallium is a large, soft metal whose atoms tend to have high coordination numbers,[63] and several compounds reported in this paper have close intra- and intermolecular

(53) Sheldrick, G. M. *SHELXTL: Program Library for Structure Solution and Molecular Graphics*, 5.10; Bruker AXS: Madison, WI, 2000.
(54) Guerra, C. F.; Snijders, J. G.; Te Velde, G.; Baerends, E. J. *Theor. Chem. Acc.* **1998**, *99*, 391−403.
(55) Te Velde, G.; Bickelhaupt, F. M.; Baerends, E. J.; Fonseca Guerra, C.; Van Gisbergen, S. J. A.; Snijders, J. G.; Ziegler, T. *J. Comput. Chem.* **2001**, *22*, 931−967.
(56) *ADF2004.01, SCM, Theoretical Chemistry*; Vrije Universiteit: Amsterdam, 2004.
(57) Vosko, S. H.; Wilk, L.; Nusair, M. *Can. J. Phys.* **1980**, *58*, 1200−11.
(58) Roesky, H. W.; Scholz, M.; Noltemeyer, M.; Edelmann, F. T. *Inorg. Chem.* **1989**, *28*, 3829−30.
(59) El-Hadad, A. A.; Kickham, J. E.; Loeb, S. J.; Taricani, L.; Tuck, D. G. *Inorg. Chem.* **1995**, *34*, 120−3.
(60) Zechmann, C. A.; Boyle, T. J.; Pedrotty, D. M.; Alam, T. M.; Lang, D. P.; Scott, B. L. *Inorg. Chem.* **2001**, *40*, 2177−2184.
(61) Kim, M.; Zakharov, L. N.; Rheingold, A. L.; Doerrer, L. H. *Polyhedron* **2005**, *24*, 1803−1812.
(62) Dahl, L. F.; Davis, G. L.; Wampler, D. L.; West, R. *J. Inorg. Nucl. Chem.* **1962**, *24*, 357−63.
(63) Cotton, F. A.; Wilkinson, G.; Murillo, C. A.; Bochmann, M. *Advanced Inorganic Chemistry*, 6th ed.; John Wiley and Sons: New York, 1999; p 1355.

Table 2. Selected Interatomic Distances, Bond Lengths, and Angles in TlOAr Compounds[a]

distances	(Å)	angles	(deg)
		1	
Tl(1)−O(1)	2.610(5)	O(1)−Tl(1)−O(2)	76.44(16)
Tl(1)−O(2)	2.583(5)	O(1)−Tl(1)− O(2_2)[b]	80.38(16)
Tl(1)−O(2_2)[b]	2.572(5)	O(2)−Tl(1)−O(2_2)[b]	74.60(17)
Tl(2)−O(1)	2.557(5)	O(1)−Tl(2)−O(1_1)[b]	73.86(17)
Tl(2)−O(1_2)[b]	2.562(5)	O(1)−Tl(2)−O(2)	76.64(15)
Tl(2)−O(2)	2.624(5)	O(1)−Tl(2)−O(2_2)[b]	80.30(15)
		Tl(1)−O(1)−Tl(2)	103.07(16)
		Tl(1)−O(1)−Tl(2_2)[b]	96.24(17)
		Tl(2)−O(1)−Tl(2_2)[b]	105.80(17)
		Tl(1)−O(2)−Tl(2)	101.95(17)
		Tl(1)−O(2)−Tl(1_1)[b]	105.16(17)
		Tl(1)−O(2)−Tl(2_2)[b]	95.63(16)
		2	
Tl(1)−O(1)	2.656(4)	O(1)−Tl(1)−O(1_2)[b]	61.82(19)
Tl(1)−O(1_2)[b]	2.844(4)	O(1)−Tl(2)−O(1_6)[b]	67.9(2)
Tl(1)−O(2)	3.196(8)	O(1)−Tl(2)−O(2)	79.65(18)
Tl(2)−O(1)	2.443(4)	O(1)−Tl(1)−Tl(1)	51.51(10)
Tl(2)−O(2)	2.684(8)	Tl(2)−O(1)−Tl(1)	102.18(16)
Tl(1)−Tl(1_2)[b]	3.5943(15)		
		2b	
Tl(1)−O(1)	2.613(5)	O(1)−Tl(1)−O(1)	81.23(17
Tl(1)−O(1)	2.672(5)	O(1)−Tl(1)−O(1)	74.50(16)
Tl(1)−O(1)	2.708(5)	O(1)−Tl(1)−O(1)	102.05(17)
O(1)−C(1)	1.315(8)	Tl(1)−O(1)−Tl(1)	105.50(16)
		Tl(1)−O(1)−Tl(1)	98.77(17)
		C(1)−O(1)−Tl(1)	116.4(4)
		C(1)−O(1)−Tl(1)	124.2(4)
		C(1)−O(1)−Tl(1)	107.8(4)
		3	
Tl(1)−O(1)	2.564(6)	O(1)−Tl(1)−O(2)	83.5(2)
Tl(1)−O(2)	2.819(6)	O(1)−Tl(1)−O(3)	81.3(2
Tl(1)−O(3)	2.906(6)	O(1)−Tl(1)−O(4)	90.9(2)
Tl(1)−O(4)	2.903(7)	O(2)−Tl(1)−O(3)	59.74(19)
		O(2)−Tl(1)−O(4)	119.3(2)
		O(3)−Tl(1)−O(4)	59.6(2)

[a] Numbers in parentheses are estimated deviations of the last significant figure. [b] Symmetry equivalent of the corresponding atom.

contacts between thallium and adjacent atoms, most often with fluorine atoms. The sum of thallium (1.96 Å) and fluorine (1.47 Å) van der Waals radii[5] is 3.43 Å. The shortest intermolecular contacts (in Å) in **1** are between the thallium atoms and fluorine atoms on the CF_3 groups: Tl(1)−F(12) 3.363(6), Tl(2)−F(2_6) 3.275(6), Tl(2)−F(2_5), and Tl(2)−F(8_7) 3.375(7) (Supporting Information, Figure S1).

Compound **2** exhibits an entirely new motif in $\{TlOAr\}_4$ chemistry. As shown in Figure 2, two thallium atoms and four oxygen atoms form the vertexes of a pseudo-octahedron. The equatorial oxygen atoms form a rectangle whose O(1)···O(1_6) sides are 2.728(8) and O(1)···O(1_2) = 3.151(8) Å in length. The remaining two thallium atoms in **2** bind two bridging aryloxide ligands with Tl(2)−O(1) bonds of 2.443(4) Å on opposite O···O edges of the pseudo-octahedron and one THF molecule with a Tl(2)−O(2) bond of 2.684(8) Å. Each THF also exhibits a very long interaction with a thallium atom at the apex of the square bipyramid. The Tl(1)···O(THF) distance of 3.196(8) Å is on the edge of reported Tl···OR_2 contacts[12] (see compound **3** below). The unit could also be described as two thallium atoms bridged by four μ_2-OAr^F ligands. Such $[M_2(\mu_2\text{-}OR)_4]$ units have been rarely seen, and we are aware of only one other crystallographically characterized example, a ditungsten(III) compound with six neopentoxide ligands (four bridging) and a W≡W triple bond.[64] A related motif has been observed with chelating ligands in $[M_2(\mu_2,\eta^2\text{-acac})_2]$ compounds with silver[65,66] and thallium.[7] The former have a noticeably short Ag···Ag distances of 2.9226(10)[66] and 3.0134(3)[65] Å consistent with argentophilicity, and the latter have thallophilic contacts averaging 3.701(4) Å.[7]

A third possible description of **2** is that of two $(TlOAr)_2$ dimers joining through two TlO_2 triangles and forming four Tl−O bonds, as shown below on the right of Scheme 1. The Tl(1)−O(1) bonds (in Å) show a slight asymmetry between Tl(1)−O(1) and Tl(1)−O(1_2) of 2.656(4) versus 2.844(4), respectively, resulting in 2-fold, not 4-fold, symmetry along the Tl···Tl vector (see Figure 2). The length of the Tl(1)−Tl(1_2) bond holding the dimers together along the axis of the pseudo-octahedron is 3.5943(15) Å and well within the range of 31 structurally characterized Tl(I)−Tl(I) bonds (3.146−3.887 Å)[12] and is one of the shortest Tl···Tl contacts in Tl(I) systems with oxygen donor atoms. The Tl(1)···Tl(2) contact is 3.9696(15) Å long and outside definitive bonding range. Figure 2 also shows the parallel arrangement of the aryloxide ligands in which the inter-ring C···C and C···F contacts are on the edge of the van der Waals distances and consistent with π-stacking. The closest inter-ring separations are C(1)···C(6_2) at 3.362(15) Å and C(5)···F(1_2) at 3.324(15) Å and would be difficult to achieve with the OAr′ ligands and their meta CF_3 groups. In **2**, the closest intramolecular Tl···F distance is 3.252(8) Å between Tl(1) and F(1) and the closest intermolecular interaction is 3.237(8) Å between Tl(2) and F(3) (Supporting Information, Figure S2).

When $TlOAr^F$ is recrystallized from CH_2Cl_2, no solvent is incorporated and an infinite ladder chain is observed, $\{TlOAr^F\}_\infty$, **2b**, as shown in Figure 3 with distance and angle information summarized in Table 2. This infinite ladder pattern has, to our knowledge, not been seen before with any metal phenolate, although the M_2O_2 quadrangle present in the $\{TlOAr^F\}_2$ units is seen in numerous dimer and cubane stuctures. Each thallium center is coordinated to three aryloxide ligands, and each aryloxide group bridges three thallium atoms with crystallographically unique distances of Tl(1)−O(1) and Tl(1)−O(1_2) equal to 2.613(5) and 2.672(5) Å respectively, with contacts to F(1) and F(6) of 3.053(4) and 3.020(4) Å as well (Supporting Information, Figure S3). The interior O(1)−Tl(1)−O(1_2) and Tl(1)−O(1)−Tl(1_2) angles are 81.23(17)° and 98.77(17)°, respectively. The Tl(1)···Tl(1) distance between every other "rung" on the ladder is 4.182 Å, and between adjacent ladder chains in the unit cell, the closest contacts are that of Tl(1) to F(1), F(2), and F(4) at 3.277(4), 3.424(5), and 3.268(4) Å, respectively (Supporting Information, Figure S3).

In the presence of 18-crown-6, all intermolecular contacts between $TlOAr^F$ units are broken and a simple mononuclear

(64) Cayton, R. H.; Chacon, S. T.; Chisholm, M. H.; Huffman, J. C. *Angew. Chem., Int. Ed. Engl.* **1990**, *29*, 1026−1028.
(65) Doppelt, P.; Baum, T. H.; Ricard, L. *Inorg. Chem.* **1996**, *35*, 1286−91.
(66) Darr, J. A.; Poliakoff, M.; Blake, A. J.; Li, W.-S. *Inorg. Chem.* **1998**, *37*, 5491−5496.

Table 3. Selected Interatomic Distances and Angles in $Tl_2Cu(OAr)_4$ Compounds[a]

distance (Å)				angle (deg)			
				4			
Tl(1)−O(1)	2.757(7)	Cu(1)−O(4)	1.929(7)	O(1)−Tl(1)−O(19)	103.5(2)	O(8)−Cu(2)−O(7)	83.0(3)
Tl(1)−O(19)	2.767(10)	Cu(2)−O(5)	1.927(7)	O(3)−Tl(3)−O(6)	101.4(2)	O(9)−Cu(3)−O(10)	83.2(3)
Tl(2)−O(2)	2.710(7)	Cu(2)−O(6)	1.937(8)	O(5)−Tl(4)−O(2)	110.9(4)	O(9)−Cu(3)−O(11)	99.6(3)
Tl(2)−O(21)	2.955	Cu(2)−O(7)	1.943(7)	O(10)−Tl(5)−O(7)	98.8(2)	O(9)−Cu(3)−O(12)	168.7(4)
Tl(3)−O(3)	2.660(7)	Cu(2)−O(8)	1.931(7)	O(9)−Tl(6)−O(8)	100.3(2)	O(10)−Cu(3)−O(12)	97.4(3)
Tl(3)−O(6)	2.702(8)	Cu(3)−O(9)	1.912(7)	O(11)−Tl(7)−O(14)	103.3(3)	O(11)−Cu(3)−O(10)	168.6(4)
Tl(4)−O(5)	2.725(8)	Cu(3)−O(10)	1.924(7)	O(12)−Tl(8)−O(13)	97.4(2)	O(11)−Cu(3)−O(12)	82.1(3)
Tl(4)−O(22)	2.738(12)	Cu(3)−O(11)	1.919(7)	O(15)−Tl(9)−O(18)	102.8(2)	O(13)−Cu(4)−O(14)	81.6(3)
Tl(5)−O(10)	2.664(8)	Cu(3)−O(12)	1.928(7)	O(1)−Cu(1)−O(2)	84.8(3)	O(13)−Cu(4)−O(15)	98.8(3)
Tl(5)−O(7)	2.716(7)	Cu(4)−O(13)	1.918(6)	O(1)−Cu(1)−O(3)	99.3(3)	O(13)−Cu(4)−O(16)	166.8(3)
Tl(6)−O(9)	2.735(8)	Cu(4)−O(14)	1.946(8)	O(1)−Cu(1)−O(4)	164.0(4)	O(15)−Cu(4)−O(14)	167.2(4)
Tl(6)−O(8)	2.763(7)	Cu(4)−O(15)	1.927(7)	O(2)−Cu(1)−O(3)	163.3(3)	O(16)−Cu(4)−O(14)	100.0(3)
Tl(7)−O(11)	2.709(8)	Cu(4)−O(16)	1.922(6)	O(4)−Cu(1)−O(2)	97.6(3)	O(16)−Cu(4)−O(15)	82.5(3)
Tl(7)−O(14)	2.755(8)	Cu(5)−O(17)	1.915(7)	O(4)−Cu(1)−O(3)	83.0(3)	O(17)−Cu(5)−O(18)	82.3(3)
Tl(8)−O(12)	2.716(8)	Cu(5)−O(18)	1.935(7)	O(5)−Cu(2)−O(6)	83.5(3)	O(17)−Cu(5)−O(19)	100.1(3)
Tl(8)−O(13)	2.749(8)	Cu(5)−O(19)	1.916(7)	O(5)−Cu(2)−O(7)	98.8(3)	O(17)−Cu(5)−O(20)	167.3(4)
Tl(9)−O(15)	2.629(8)	Cu(5)−O(20)	1.916(7)	O(5)−Cu(2)−O(8)	163.8(4)	O(19)−Cu(5)−O(18)	167.6(4)
Tl(9)−O(18)	2.654(7)	Tl(1)···Tl(2)	3.936(1)	O(6)−Cu(2)−O(7)	167.6(4)	O(19)−Cu(5)−O(20)	83.1(3)
Tl(10)−O(17)	2.746(8)	Tl(3)···Tl(4)	3.851(1)	O(8)−Cu(2)−O(6)	98.2(3)	O(20)−Cu(5)−O(18)	97.3(3)
Tl(10)−O(16)	2.862	Tl(5)···Tl(6)	3.914(1)				
Cu(1)−O(1)	1.907(7)	Tl(7)···Tl(8)	3.786(1)				
Cu(1)−O(2)	1.934(7)	Tl(9)···Tl(10)	3.893(1)				
Cu(1)−O(3)	1.953(8)						
				5			
Tl(1)−O(1)	2.514(5)	Tl(2)−O(4_3)[c]	2.643(4)	O(2)−Tl(1)−O(1)−	61.27(15)	O(1)−Cu(1)−O(3)	99.20(19)
Tl(1)−O(1S)[b]	2.641(14)	Tl(2)···Tl(2)	3.5643(5)	O(2)−Tl(1)−O(1S)[b]	79.2(3)	O(2)−Cu(1)−O(4)	98.27(19)
Tl(1)−O(2)	2.512(4)	Cu(1)−O(1)	1.914(4)	O(1)−Tl(1)−O(1S)[b]	79.5(3)	O(1)−Cu(1)−O(4)	166.8(2)
Tl(2)−O(3)	2.648(5)	Cu(1)−O(2)	1.914(5)	O(4)−Tl(2)−O(3)	101.72(14)	O(3)−Cu(1)−O(4)	81.70(19)
Tl(2)−O(4)	2.857(4)	Cu(1)−O(3)	1.938(4)	O(4)−Tl(2)−O(3)	56.40(13)	Cu(1)−O(1)−Tl(1)	106.5(2)
Tl(2)−O(3_3)[c]	2.730(4)	Cu(1)−O(4)	1.945(4)	O(3)−Tl(2)−O(3)	73.99(16)	Cu(1)−O(2)−Tl(1)	106.57(19)
				O(4)−Tl(2)−Tl(2)	52.28(10)	Cu(1)−O(3)−Tl(2)	102.02(18)
				O(3)−Tl(2)−Tl(2)	49.49(9)	Cu(1)−O(3)−Tl(2)	96.85(16)
				O(3)−Tl(2)−Tl(2)	47.51(10)	Tl(2)−O(3)−Tl(2)	83.00(12)
				O(2)−Cu(1)−O(1)	84.0(2)	Cu(1)−O(4)−Tl(2)	99.56(17)
				O(2)−Cu(1)−O(3)	166.3(2)		
				5b			
Tl(1)−O(1)	2.519(5)	Cu(1)−O(1)	1.899(5)	O(2)−Tl(1)−O(1)	61.17(17)	Cu(1)−O(1)−Tl(1)	107.3(2)
Tl(1)−O(2)	2.506(5)	Cu(1)−O(2)	1.915(5)	O(2)−Tl(1)−O(3)	93.6(3)	Cu(1)−O(2)−Tl(1)	107.3(2)
Tl(1)−O(3)	2.774(10)			O(1)−Tl(1)−O(3)	97.9(3)	C(1)−O(1)−Tl(1)	122.6(5)
				O(1)−Cu(1)−O(1_3)[c]	98.7(3)	C(9)−O(2)−Tl(1)	125.1(5)
				O(1)−Cu(1)−O(2_3)[c]	165.2(3)	C(1)−O(1)−Cu(1)	128.8(5)
				O(1)−Cu(1)−O(2)	84.2(2)	C(9)−O(2)−Cu(1)	125.4(5)
				O(2)−Cu(1)−O(2_3)[c]	96.7(3)		

[a] Numbers in parentheses are estimated deviations of the last significant figure. [b] O(1S) is the O atom of the solvent THF molecule. [c] Symmetrical equivalent of the corresponding atom.

species, **3**, results in which the thallium atom is heptacoordinated to oxygen atoms: six from the crown ether and one from the aryloxide. As shown in Figure 4, the thallium center is slightly displaced out of the plane of the six ether oxygen atoms but the average Tl−O distance, 2.97(11) Å, is otherwise unexceptional. The Tl(1)···F(12) distance is 3.109(6) Å.

Previously, our group reported the syntheses and spectroscopic characterization[50] of $Tl_2Cu(OAr^F)_4$, **4**, and $Tl_2Cu(OAr')_4$, **5**, whose structures are now described. To our knowledge, there is only one other example of a structurally characterized thallium aryloxide bimetallic (thallium and titanium) compound.[67] When recrystallized from C_6D_6/d_8-THF, compound **4** reveals a unique helical chain, as shown in Figure 5. The asymmetric unit has the stoichiometry $[Tl_2Cu(OAr^F)_4]_5 \cdot 2THF \cdot 4C_6D_6$, but the helix has an infinite extent through the crystal such that Tl(1) and Tl(2) also coordinate to the O(19) and O(20) atoms in the next unit cell. All aryloxide oxygen atoms in the helix chain are μ_2-bridges between copper and thallium atoms such that adjacent $Cu(\mu_2\text{-}OAr^F)_4$ units are joined by two thallium atoms. Thus, four oxygen and two thallium atoms form a distorted octahedron with oxygen atoms in equatorial and thallium atoms in apical positions. The coordination geometry features for each of the five copper atoms in the asymmetric unit are similar; therefore, only the first will be discussed in detail, and the analogous parameters for the other four centers may be found in Table 3. The distorted square-planar center Cu(1) is bound to four aryloxide groups via O(1), O(2), O(3), and O(4), as shown in Figure 6, and every aryloxide group is also a bridging ligand to a thallium atom. The average Cu(1)−O distance is 1.931(19) Å, and the other copper centers have highly similar coordination environments (Table 3). The $\{Tl_2(\mu_2\text{-}OAr)_4\}$ pseudo-octahedron unit made of Tl(3), Tl(4), O(3), O(4), O(5), and O(6) bridges the Cu(1) and Cu(2) centers. The dihedral angle at Cu(1) defined by

(67) Boyle, T. J.; Zechmann, C. A.; Alam, T. M.; Rodriguez, M. A.; Hijar, C. A.; Scott, B. L. *Inorg. Chem.* **2002**, *41*, 946−957.

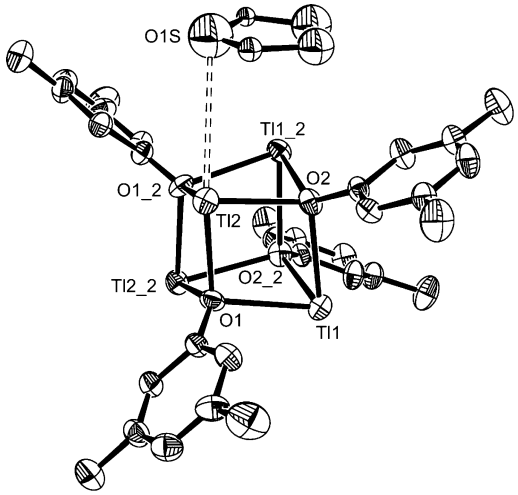

Figure 1. ORTEP of **1** with hydrogen and fluorine atoms removed for clarity and ellipsoids at the 50% level. Selected bond lengths (Å) and angles (deg): Tl(1)−O(1) 2.610(5), Tl(1)−O(2) 2.583(5), Tl(1)−O(2_2) 2.572(5), Tl(2)−O(1) 2.557(5), Tl(2)−O(1_2) 2.562(5), Tl(2)−O(2) 2.624(5), O(1)−Tl(1)−O(2) 76.44(16), O(1)−Tl(1)−O(2_2) 80.38(16), O(2)−Tl(1)−O(2_2) 74.60(17), O(1)−Tl(2)−O(1_1) 73.86(17), O(1)−Tl(2)−O(2) 76.64(15), O(1)−Tl(2)−O(2_2) 80.30(15), Tl(1)−O(1)−Tl(2) 103.07(16), Tl(1)−O(1)−Tl(2_2) 96.24(17), Tl(2)−O(1)−Tl(2_2) 105.80(17), Tl(1)−O(2)−Tl(2) 101.95(17), Tl(1)−O(2)−Tl(1_1) 105.16(17), Tl(1)−O(2)−Tl(2_2) 95.63(16).

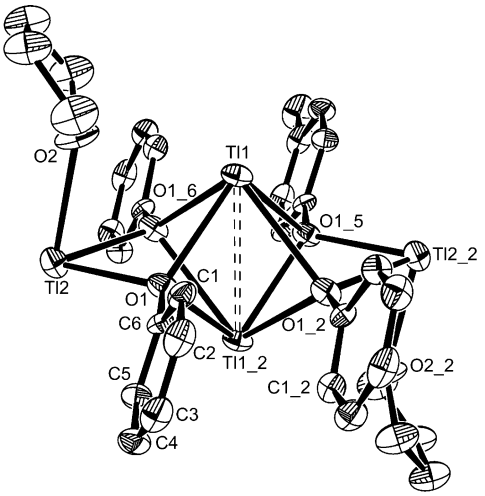

Figure 2. ORTEP of **2** with hydrogen and fluorine atoms removed for clarity and ellipsoids at the 50% level. A mirror plane relates O(1) and O(1_6) and a 2-fold axis relates O(1) and O(1_5). Selected bond lengths (Å) and angles (deg): Tl(1)−O(1) 2.656(4), Tl(1)−O(1_2) 2.844(4), Tl(1)−O(2) 3.196(8), Tl(2)−O(1) 2.443(4), Tl(2)−O(2) 2.684(8), Tl(1)−Tl(1_2) 3.5943(15), O(1)−Tl(1)−O(1_2) 61.82(19), O(1)−Tl(2)−O(1_6) 67.9(2), O(1)−Tl(2)−O(2) 79.65(18), O(1)−Tl(1)−Tl(1) 51.51(10), Tl(2)−O(1)−Tl(1) 102.18(16).

Scheme 1

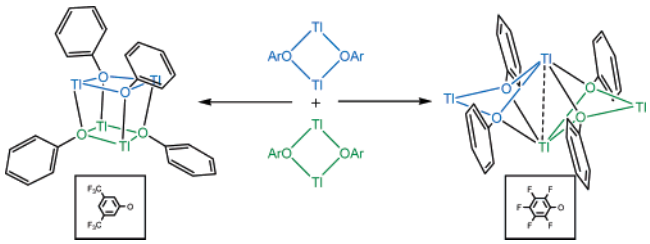

the O(1)Cu(1)O(2) and O(3)Cu(1)O(4) planes is 24.5°, and the analogous dihedral angles at Cu(2),Cu(3), Cu(4) and Cu(5) are 21.8°, 17.1°, 19.8°, and 18.9°, respectively. The

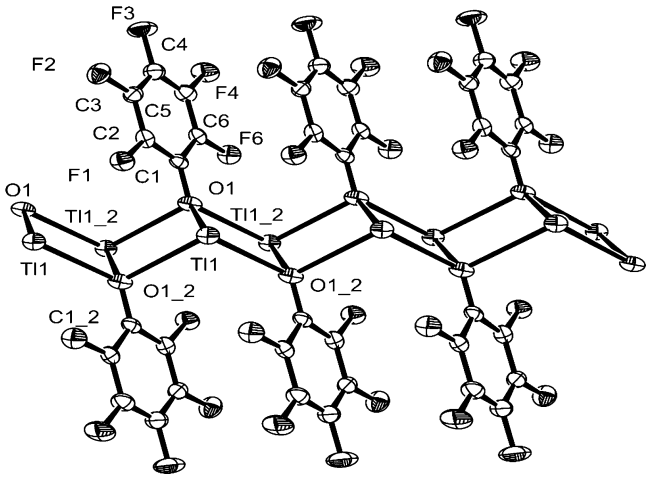

Figure 3. ORTEP of **2b** with ellipsoids at the 50% level. Selected bond lengths (Å) and angles (deg): Tl(1)−O(1) 2.613(5), Tl(1)−O(1_2) 2.672(5), O(1)−Tl(1)−O(1_2) 81.23(17), Tl(1)−O(1)−Tl(1_2) 98.77(17).

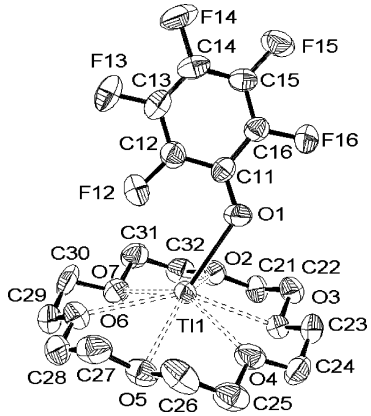

Figure 4. ORTEP of **3** with hydrogen atoms removed for clarity and ellipsoids at the 50% level. Selected bond lengths (Å) and angles (deg): Tl(1)−O(1) 2.564(6), Tl(1)−O(2). 2.819(6), Tl(1)−O(3) 2.906(6), Tl(1)−O(4) 2.903(7), O(1)−Tl(1)−O(2) 83.5(2), O(1)−Tl(1)−O(3) 81.3(2), O(1)−Tl(1)−O(4) 90.9(2), O(2)−Tl(1)−O(3) 59.74(19), O(2)−Tl(1)−O(4) 119.3(2), O(3)−Tl(1)−O(4) 59.6(2).

dihedral angle between the planes defined by O(3)Cu(1)O-(4) and O(5)Cu(2)O(6) is 17.6°, and the other three such angles are 19.5°, 13.1°, 15.4°, and 20.5° is the angle between the planes defined by O(1)−Cu(1)−O(2) and O(19)−Cu(5)−O(20) in adjacent asymmetric units. The angle between the Tl···Tl vector and a normal to the average plane of the (μ_2-O)$_4$ fragment in each {Cu(μ_2-O)$_4$Tl$_2$}$_n$ unit is in the range 2.2−2.9°. The Tl···Tl contacts in each {Tl$_2$(μ_2-O$_4$)} unit in **4** average 3.86(6) Å and are thus longer than the analogous contact in **2** and that in **5** (vide infra) but less than the van der Waals radii sum.

The central {Cu(μ_2-O)$_4$Tl$_2$}$_n$ core in the chain is surrounded by C_6F_5 groups and coordinated C_6D_6 and THF solvent molecules (Figure 5) such that several thallium atoms in **4** are bonded also to benzene or THF molecules. The two THF molecules are η^1-coordinated to Tl(2) and Tl(4), and the atoms Tl(1), Tl(6), Tl(8), and Tl(10) are coordinated in an η^6-fashion to benzene molecules with average Tl−C distances of 3.42(5), 3.53(6), 3.42(6), and 3.42(6) Å, respectively. Arene coordination to M(I) Group 13 metals

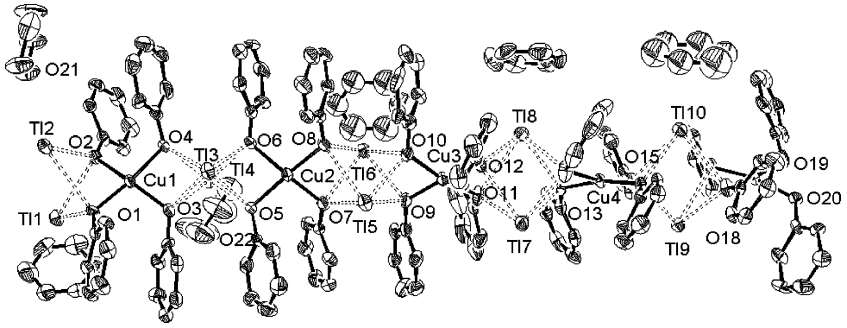

Figure 5. ORTEP of **4** with hydrogen and fluorine atoms removed for clarity and ellipsoids drawn at the 35% probability level. Selected bond lengths (Å) and angles (deg): Tl(1)−Tl(2) 3.936(1), Tl(3)−Tl(4) 3.851(1), Tl(5)−Tl(6) 3.914(1), O(3)−Tl(3)−O(6) 101.4(2), O(5)−Tl(4)−O(2) 110.9(4), O(10)−Tl(5)−O(7) 98.8(2), O(9)−Tl(6)−O(8) 100.3(2).

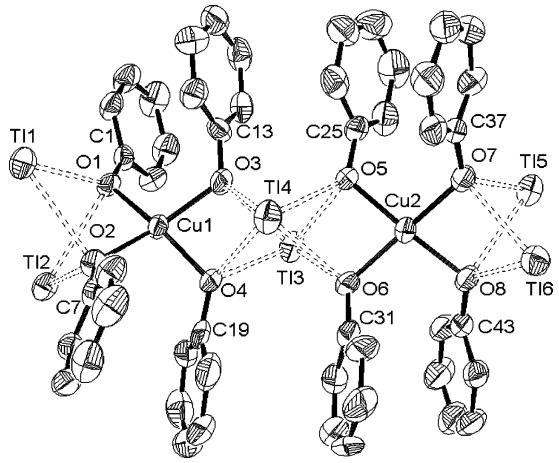

Figure 6. ORTEP of two $[Cu(OAr^F)_4]$ units and bridging thallium atoms in **4** with hydrogen and fluorine atoms and solvent molecules removed for clarity. Ellipsoids drawn at the 50% probability level. Selected bond lengths (Å) and angles (deg): Cu(1)−O(1) 1.907(7), Cu(1)−O(2) 1.934(7), Cu(1)−O(3) 1.953(8), Cu(1)−O(4) 1.929(7), O(1)−Cu(1)−O(2) 84.8(3), O(1)−Cu(1)−O(3) 99.3(3), O(1)−Cu(1)−O(4) 164.0(4), O(2)−Cu(1)−O(3) 163.3(3), O(4)−Cu(1)−O(2) 97.6(3), O(4)−Cu(1)−O(3), 83.0(3).

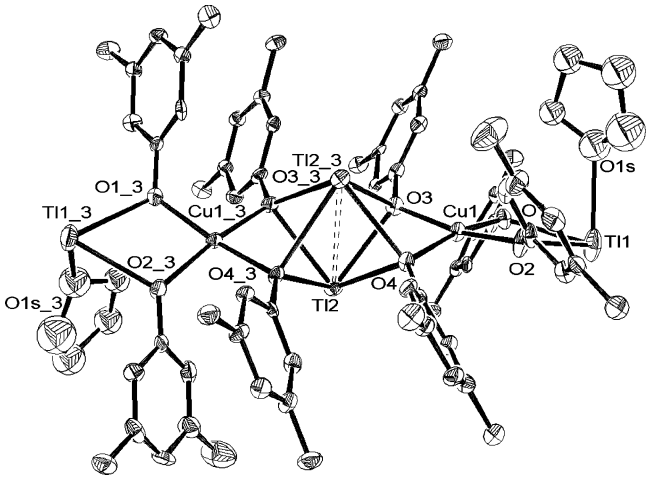

Figure 7. ORTEP of **5** with hydrogen and fluorine atoms removed for clarity and ellipsoids drawn at the 50% probability level. Selected bond lengths (Å) and angles (deg): Tl(1)−O(1) 2.514(5), Tl(1)−O(1S) 2.641(14), Tl(1)−O(2) 2.512(4), Tl(2)−O(3) 2.730(4), Tl(2)−O(4) 2.643(4), Cu(1)−O(1) 1.914(4), Cu(1)−O(2) 1.914(5), Cu(1)−O(3) 1.938(4), Cu(1)−O(4) 1.945(4).

including thallium is well precedented.[68] The remaining four thallium atoms are coordinated, in addition to the bridging aryloxide groups, intramolecularly to fluorine atoms at distances less than 3.5 Å as follows. Tl(3) to F(15) and F(26); Tl(5) to F(25), F(35), F(46), and F(56); Tl(7) to F(55) and F(66); and Tl(9) to F(75) and F(86). There are also intermolecular Tl−F contacts less than 3.5 Å between Tl(5) and F(23); Tl(7) and F(13); and Tl(9) and F(98) (Supporting Information, Figure S4).

The crystal structure of $[Tl_2Cu(OAr')_4]$, **5**, also displays a bridging $\{Tl_2(\mu_2\text{-}OAr)_4\}$ unit, as shown in Figure 7, but in this case, the Tl···Tl contact is significantly shorter at 3.564(1) Å than those in compound **4**. This close contact is particularly interesting in comparison to the structure of **2** because it demonstrates that the bulkier OAr′ ligands do not prevent a bridging $\{Tl_2(\mu_2\text{-}O)_4\}$ unit from forming in **1**. The bridging aryloxide Tl−O distances average 2.72(10) Å and are slightly asymmetric as viewed down the Tl(2)···Tl(2_3) vector, as can be seen in Figure 7 and Table 3. The terminal thallium atom has an average distance of 2.513(15) Å to the aryloxide oxygen atoms and slightly longer distance of 2.641(14) Å to the solvent oxygen atom. The angle between the Tl···Tl line and a normal to the average plane of the $(\mu_2\text{-}O)_4$ fragment in the $Cu(\mu_2\text{-}O)_4Tl_2$ unit in **5** is 1.8°. Each THF solvate molecule is noticeably oriented away from the Tl(1)···Tl(1_3) vector, suggesting a sterically active thallium lone pair on each terminal thallium, similar to that indicated for **1** by DFT calculations as shown in Figure S8, vide infra. The only Tl···F contacts shorter than 3.5 Å are intermolecular ones to Tl(1) by F(12) and F(13) at 3.456 and 3.483 Å, respectively, and between Tl(2) and F(5), F(20), and F(21) at an average distance of 3.44(8) Å (Supporting Information, Figure S5). It is noted that no helix structure like that of **4** is observed in **5**. This could be due in **5** to an absence of aromatic ring π-stacking or the stabilizing influence of the solvating benzene molecules. No crystals of **5** were able to be grown from aromatic solvents.

We note that a similar $\{Tl_2(\mu_2\text{-}S)_4\}$ motif was structurally characterized in several chelating dithiocarbamate dimers some years ago, $[Tl(S_2CN(^iPr)_2)]_2$,[69] $[Tl(S_2CN(Me)_2)]_2$,[70] $[Tl(S_2CN(^nBu)_2)]_2$,[71] and $[Tl(S_2CN(Et)_2)]_2$[72,73] with intramo-

(68) Schmidbaur, H. *Angew. Chem.* **1985**, *97*, 893−904.

(69) Jennische, P.; Olin, A.; Hesse, R. *Acta Chem. Scand.* **1972**, *26*, 2799−812.

(70) Jennische, P.; Hesse, R. *Acta Chem. Scand.* **1973**, *27*, 3531−44.

(71) Elfwing, E.; Anacker-Eickhoff, H.; Jennische, P.; Hesse, R. *Acta Chem. Scand.* **1976**, *A30*, 335−9.

(72) Pritzkow, H.; Jennische, P. *Acta Chem. Scand. A* **1975**, *A29*, 60−70.

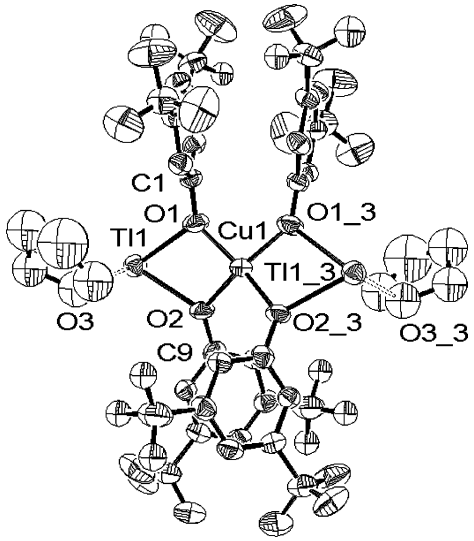

Figure 8. ORTEP of **5b** with hydrogen and fluorine atoms removed for clarity and ellipsoids drawn at the 50% probability level. Selected bond lengths (Å) and angles (deg): Tl(1)−O(1) 2.519(5), Tl(1)−O(2) 2.506(5), Tl(1)−O(3) 2.774(10), Cu(1)−O(1) 1.899(5), Cu(1)−O(2) 1.915(5), O(2)−Tl(1)−O(1) 61.17(17), O(1)−Cu(1)−O(1_3) 98.7(3), O(1)−Cu(1)−O(2_3) 165.2(3), O(1)−Cu(1)−O(2) 84.2(2), O(2)−Cu(1)−O(2_3) 96.7(3).

lecular Tl···Tl contacts of 3.584(5), 3.847(6), 3.62(1), and 3.661(6) Å, respectively. These dimers were not discussed in terms of thallophilic interactions, although the short Tl···Tl distances were noted at the time and later.[74] Such interactions were included in a review of strong s^2-s^2 interactions and described as "an interesting case" by Pyykkø in a subsequent review article.[1]

A different solvate of $[Tl_2Cu(OAr')_4]$, a monomer, **5b**, has also been characterized in which every thallium is coordinated by one molecule of THF, as shown in Figure 8, and no $\{Tl_2O_4\}$ bridging unit, and therefore no thallophilic interaction, is present. The pseudo-square planar Cu(II) center has a dihedral angle of 14.7° with an average Cu(1)−O distance of 1.908(11) Å and both the Tl−OAr distances and the Tl−O(THF) distance are unremarkable compared to those of the terminal thallium atoms in **5**. The most notable feature of the compound is the orientation of the THF molecule with respect to the Tl(1)−O(1)−O(2) plane such that there is again suggestive evidence for a sterically active lone pair of $6s^2$ electrons on thallium. The orientation of the THF molecule could also be due to steric repulsion of other groups in the unit cell. There are intermolecular contacts between Tl(1) and F(1), F(5), F(6), and F(12) at an average distance of 3.31(17) Å (Supporting Information, Figure S6).

^{205}Tl and ^{203}Tl NMR Spectroscopy. Solution-state thallium NMR spectroscopy was used to assess the stability of the $(TlOAr)_4$ units in solution. Spectra were also collected on solutions containing TlOAr′, **1**, or $TlOAr^F$, **2**, with more than 1 equiv of 18-crown-6 per thallium. Both ^{203}Tl and ^{205}Tl isotopes (29.5 and 70.5% abundant, respectively) are $I = 1/2$ nuclei and have excellent sensitivity compared to ^{13}C (762 and 311 times greater, respectively).[75,76] Thallium alkoxide cubanes have been studied previously by this technique.[60,77] The chemical shifts observed at room temperature are summarized in Table 4. For both **1** and **2**, there are clear differences in the chemical shifts for samples with and without the chelating crown ether. Both samples exhibit significantly larger chemical shifts in the absence of the crown ether, with the chemical shifts being larger for the compounds in dissolved in C_6D_6 than d_6-acetone. The ^{205}Tl NMR chemical shift for **2** is consistently smaller than that for **1** (for both benzene and acetone), revealing an increase in the shielding for the thallium environment in **2**.

Table 4. ^{205}Tl NMR Chemical Shift Data[a]

Ar in TlOAr	compound	δ in C_6D_6	δ in d_6-acetone (^2J Hz)	δ in CD_2Cl_2 + 1 equiv 18-crown-6
OAr′	**1**	+ 1271	+ 1120	+ 150
			+1180 (−90 °C), J = 1125 Hz	
OAr^F	**2**	+ 1046	+ 950	+ 675
OC_6H_5	**6**			+ 36.9
2,6-$OC_6H_3(CH_3)_2$	ref 50	+ 1999[b]		
2,6-$OC_6H_3(^iPr)_2$	ref 50		+ 1850[c]	

[a] Chemical shifts with respect to 0.001 M $Tl(NO_3)$ in D_2O ($\delta = 0.0$) at 25 °C. [b] Recorded in d_8-toluene. [c] Recorded in d_8-THF.

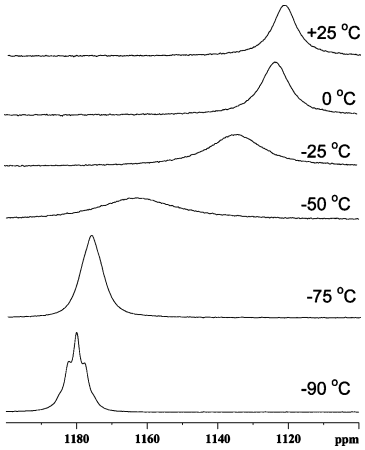

Figure 9. Variable-temperature ^{205}Tl NMR spectra of **1** in d_6-acetone.

The dynamic behavior of complex **1** in acetone solution was studied using variable-temperature (VT) NMR between +25 and −90 °C, as shown in Figure 9. At low temperatures, the J-coupling between ^{205}Tl and ^{203}Tl nuclei within the compound is clearly visible, supporting the argument for retention of the $(TlOAr')_4$ cubane structure in solution. With increasing temperatures, this J-coupling fine structure is averaged away, revealing a fluxional process that is on the NMR time scale of $\sim 1/J$ (900 μs). Recall that only a single ^{205}Tl resonance is observed in the NMR spectrum such that J-coupling between different ^{205}Tl nuclei within the cluster is not present. The J-coupling observed experimentally is between ^{205}Tl and ^{203}Tl nuclei within the cluster. Although

(73) Hong, S.-H.; Jennische, P. *Acta Chem. Scand.* **1978**, *A32*, 313−18.
(74) Janiak, C.; Hoffmann, R. *J. Am. Chem. Soc.* **1990**, *112*, 5924−46.
(75) Iggo, J. A. *NMR Spectroscopy in Inorganic Chemistry*; Oxford University Press: New York, 1999; p 90.
(76) Hinton, J. F.; Metz, K. R.; Briggs, R. W. *Prog. Nucl. Magn. Res. Spec.* **1988**, *20*, 423−513.
(77) Burke, P. J.; Matthews, R. W.; Gillies, D. G. *J. Chem. Soc., Dalton Trans.* **1980**, 1439−1442.

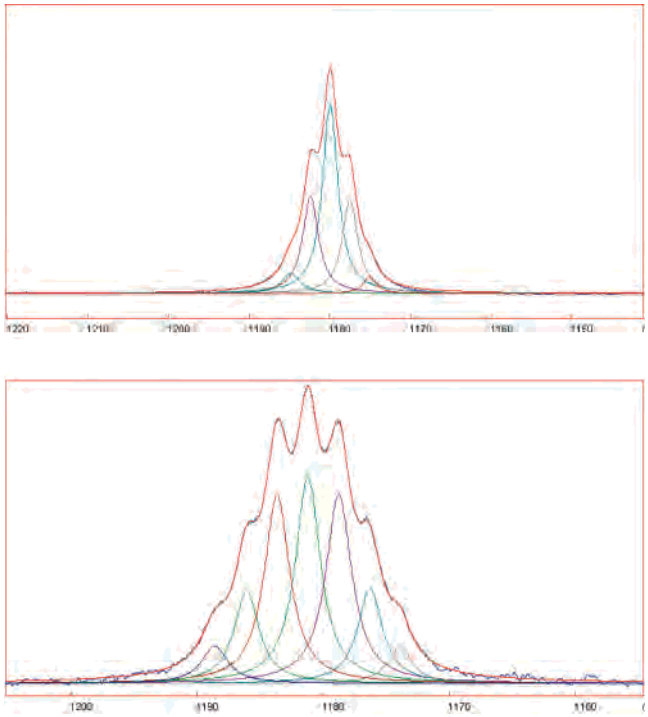

Figure 10. Deconvolution of ^{205}Tl (above) and ^{203}Tl (below) spectra of **1** in acetone at −90 °C.

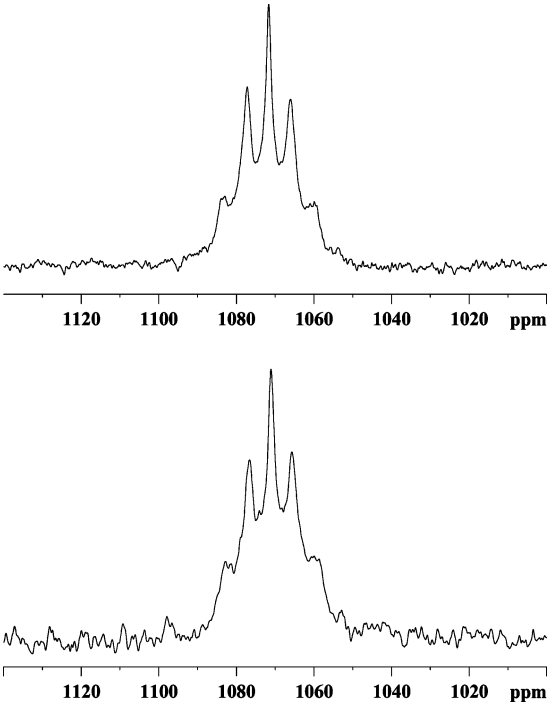

Figure 11. Spectra of **2** in CD_2Cl_2 ^{205}Tl (top) and ^{203}Tl (bottom) at −75 °C.

the ^{205}Tl NMR spectra are typically collected because of the higher natural abundance, we also have collected the ^{203}Tl NMR spectra at −90 °C because we have found that *J*-coupling fine structure is more discernible because of the higher natural abundance of the coupled nuclei (in this case ^{205}Tl), as shown in Figure 10. For example, in the ^{205}Tl NMR spectra, the ratio of the central and the first *J*-coupled resonance is ∼1.9, consistent with the predicted ratio for a tetramer cluster of 1.9; for the ^{203}Tl NMR spectra, the ratio between the central and first *J*-coupled resonance is predicted to be 1.1, whereas a ratio of 1.1 was observed experimentally. Here it is assumed that the different ^{205}Tl−^{203}Tl couplings present within the structure are all equivalent. It is possible that for **1** that there are different *J*-couplings due to the distorted cubane arrangement. The experimental Tl NMR does not reveal different *J*-couplings. A small distribution in *J*-couplings would produce a slight broadening of the observed multiplet structure due to the overlap of the different subspectra. The measured *J*-coupling for **1** is ∼1120 Hz, smaller than the 2350−2580 Hz *J*-couplings of the thallium alkoxide cubanes previously reported.[60] Deconvolution of both low-temperature spectra are shown in Figure 10 with the different sub-spectra that arise from the different isotope combinations within the cubane structure.

Similar ^{205}Tl NMR spectra were collected for **2** in acetone, but no fine structure or Tl−Tl coupling could be resolved over the temperature range investigated (Supporting Information, Figure S7). When crystals of **2** with the coordinated THF molecules were dissolved in CD_2Cl_2, the ^{205}Tl NMR spectra revealed very broad signals (∼17 000 Hz) at room temperature, but the *J*-coupling fine structure could be observed at −75 °C, shown in Figure 11, demonstrating the retention of a thallium cluster in solution. The fine structure is not consistent with a simple cubic Tl cluster in comparison to the Tl NMR of **1** in Figure 10. For **2**, the ratio of the central to first *J*-coupled resonance in the ^{205}Tl NMR spectrum is ∼1.5 versus the 1.9 predicted for a perfect cubane structure and ∼1.45 versus the predicted 1.1 for the ^{203}Tl NMR spectrum. In addition, the *J*-coupling is ∼1995 Hz, slightly larger than that observed in **1.** The Tl NMR spectra in Figure 11 demonstrate the presence of multiple Tl−Tl couplings within **2,** arguing for retention of a cluster structure. The nontypical fine structure (ratios) would suggest that the observed experimental spectra likely represents the overlap of subspectra produced by multiple and different Tl−Tl couplings within this compound. No unique deconvolution of these different sub-spectra has been obtained.

Previous work established a relationship between the pK_a of an alcohol or phenol and the ^{205}Tl chemical shift.[60] The data for **1** and **2** (pK_a values 8.26 and 8.42, respectively[78]) are consistent with this trend. Related data for thallium aryloxides are reproduced in Table 4 for comparison. Notably in previous ^{205}Tl and ^{203}Tl NMR spectra for nonfluorinated aryloxides, no Tl···Tl coupling was observed and a lower limit of 2.5 kHz was established for any fluxional process.[60]

The nonfluorinated phenoxide $TlOC_6H_5$, **6**, was also studied to understand further the electronic effect of the aryloxide group. The solubility of TlOPh in either C_6D_6 or d_6-acetone was insufficient to obtain any solution Tl NMR spectra. An NMR signal was observed in the presence of 1 equiv of 18-crown-6, as tabulated in Table 4. This chemical shift is downfield of the signals for both **1** and **2** complexed with 18-crown-6, consistent with the trend (vide supra) in ^{205}Tl NMR signals for cubane structures as a function of

(78) Abraham, M. H.; Duce, P. P.; Morris, J. J.; Taylor, P. J. *J. Chem. Soc., Faraday Trans. 1* **1987**, *83*, 2867−81.

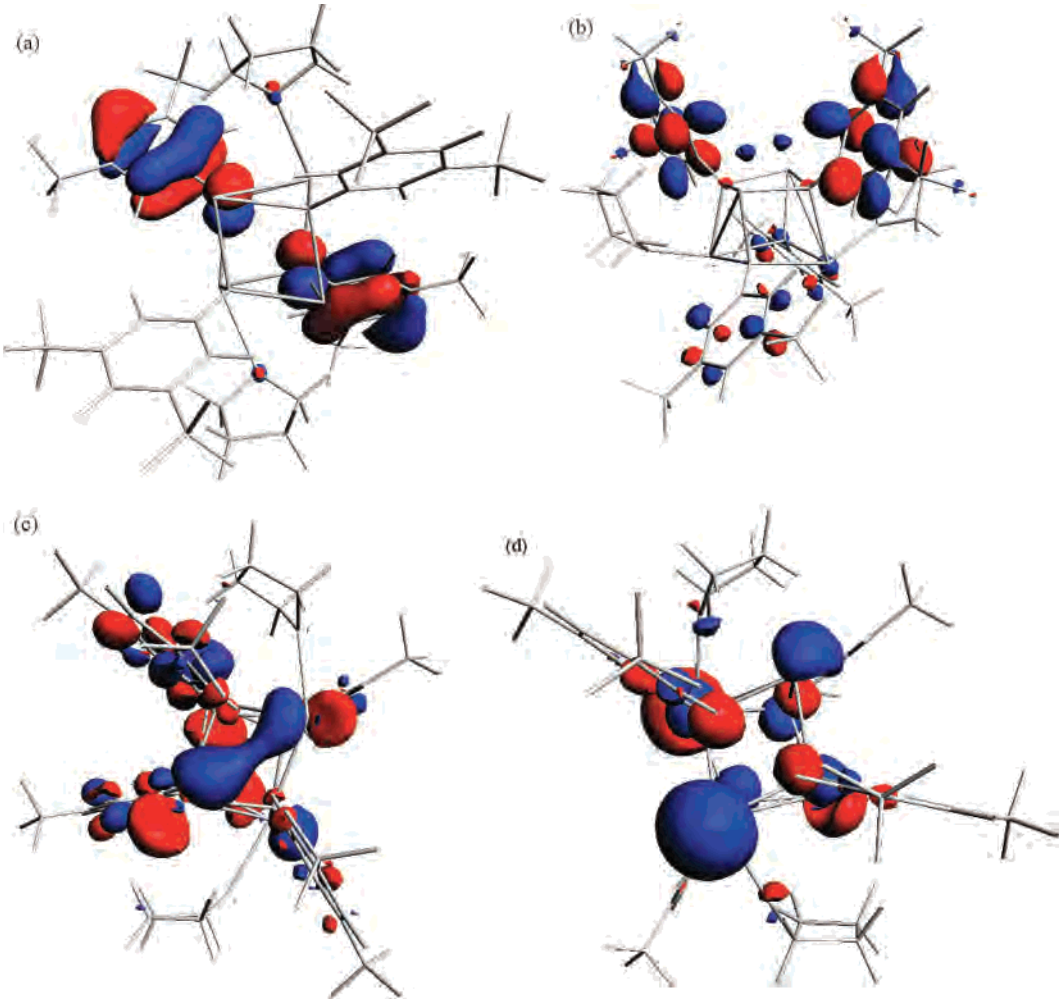

Figure 12. Molecular orbital representations (energies in eV) from DFT calculation of **1b:** (a) HOMO 214b (−6.3063), (b) LUMO 215a (−3.0688), (c) unoccupied Tl $6p_y$ bonding orbital LUMO+8 218b (−2.1543), and (d) occupied Tl 6s HOMO−4 212b (−6.6409). All orbitals are shown at the 0.03 $e^-/Å^3$ level.

Scheme 2

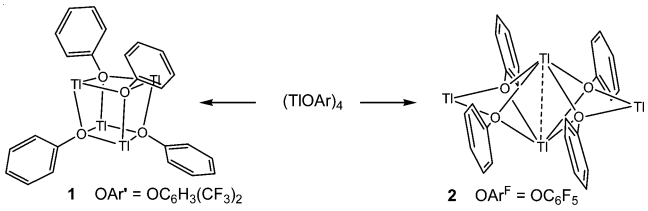

Scheme 3

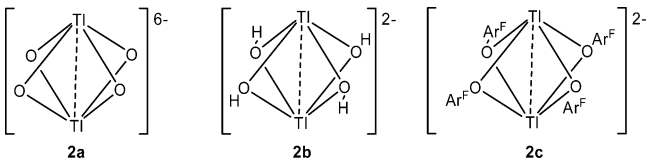

phenolic pK_a (pK_a(HOPh) = 9.78[78]). No crystallographic information is available for $Tl(OC_6H_5)$ systems except the Tl(III) compound $[Tl(OPh)(CH_3)_2]$.[79] Extremely thin needles of TlOPh were grown by recrystallization but were too small for X-ray diffraction with a Mo Kα source.

(79) Burke, P. J.; Gray, L. A.; Hayward, P. J. C.; Matthews, R. W.; McPartlin, M.; Gillies, D. G. *J. Organomet. Chem.* **1977**, *136*, C7−C10.

DFT Calculations. We have used electronic structure calculations to understand the orbital basis for the unusual structure in the $\{Tl(OAr)\}_4$ unit of **2**. In both **1** and a **2** each aryloxide bridges three thallium atoms, but there is a distinct thallium−thallium interaction in **2**, as demonstrated experimentally, vide supra, and no thallium−thallium bonding interaction in **1** (Scheme 2).

Unquestionably, the covalent bonding between thallium and the bridging aryloxides is the primary force holding each tetramer together. Metallophilicity may also play a role, however, as suggested previously: "...ligand−ligand interactions or packing effects provide for the general structural arrangement..., but...M^I−M^I bonding can be responsible for...a shift in equilibrium geometry."[74] Compound **2** exhibits two unusual features for which we wanted to understand the orbital basis: the short Tl···Tl distance and the cant of the plane of the aryloxide rings away from the Tl···Tl vector (the plane of each phenyl ring makes an angle of 74.3° to the best O_4 plane). Atomic positions from the crystal structures were used for all-electron, geometry-optimized calculations of **1b** (**1** with two THF molecules to increase the symmetry) and **2**. Three model compounds of **2** were

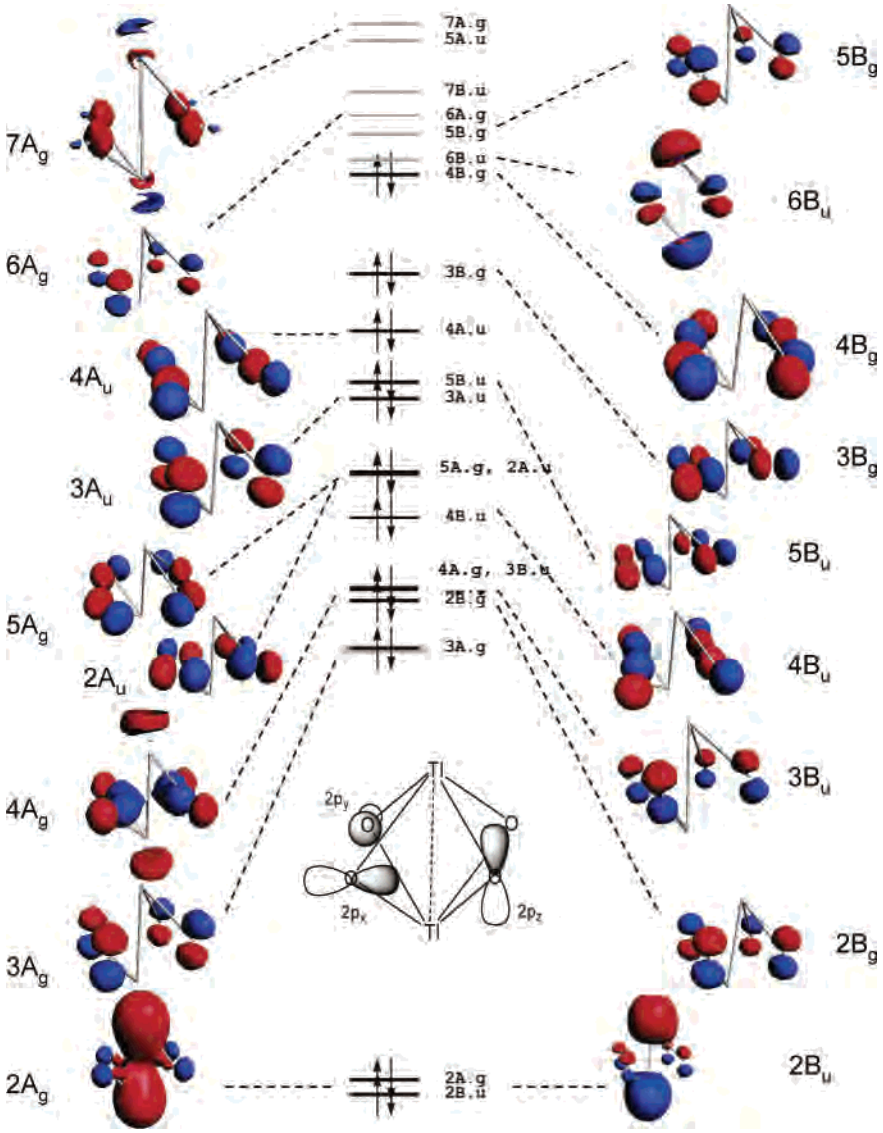

Figure 13. Molecular orbital diagram of model **2a**, $[Tl_2(\mu_2\text{-}O)_4]^{6-}$. The obital representations are shown at the 0.05 $e^-/Å^3$ level.

also studied: $\{Tl_2(\mu_2\text{-}O)_4\}^{6-}$, **2a**, $\{Tl_2(\mu_2\text{-}OH)_4\}^{2-}$, **2b**, and $\{Tl_2(\mu_2\text{-}OAr^F)_4\}^{2-}$, **2c**, as shown in Scheme 3.

The geometry-optimized structure of the calculated cubane **1b** with two coordinated THF molecules (C_2 symmetry) is in excellent agreement with the crystallographically determined structure. For example, the Tl···Tl contacts (Å) and the O−Tl−O angles (deg) in the crystal average 4.02(11) and 77(2) versus 3.93(10) and 75.5 (1.8) in the computed structure. Figure 12a and b show the ligand-based HOMO (214b) and LUMO (215a), respectively. No strong Tl···Tl overlaps are evident in the bonding orbitals. A full electron-volt above the LUMO there are in-phase Tl overlaps of empty 6p orbitals, as shown in Figure 12c. The thallium corners have localized, occupied 6s orbitals (lone pairs) that point away from the cube and force the THF solvent molecules to bind away from the Tl···O cube body diagonal, as shown in Figure 12d. A DFT calculation on **1**, the same compound but with only one THF bound as observed in the crystal structure, shows essentially the same results as the more symmetric system. The higher occupied MOs are ligand based, and the lower unoccupied MOs are also ligand based within 0.7 eV of the LUMO.

The calculation of $[Tl_2(\mu_2\text{-}O)_4]^{2-}$, **2a,** exhibits the primary bonding features of the $\{Tl_2(\mu_2\text{-}OAr^F)_4\}^{2-}$ unit and allows them to be visualized more readily in the absence of substituents on the oxygen atoms. These features are observed also in the two more detailed models and the full calculation of **2**. The MO diagram of **2a** is shown in Figure 13, in which it can be seen that the O 2s orbitals are too low in energy to interact significantly with the Tl 6s orbitals. The latter overlap best with two of the three O 2p orbitals, as illustrated on the nuclear framework in Figure 13 with each oxygen 2p orbital shown on a different atom for clarity. The O $2p_y$ orbitals along the O−C bonds have the wrong symmetry and are too distant to interact with the Tl 6s orbitals. The in-phase Tl 6s combination overlaps with the oxygen p orbitals ($2p_x$) approximately perpendicular (see sketch in Figure 13) to the Tl···Tl vector in the a_g-type orbitals ($2a_g$, $4a_g$, $7a_g$), and the out-of-phase Tl 6s combination overlaps with the oxygen p orbitals ($2p_z$) parallel to the

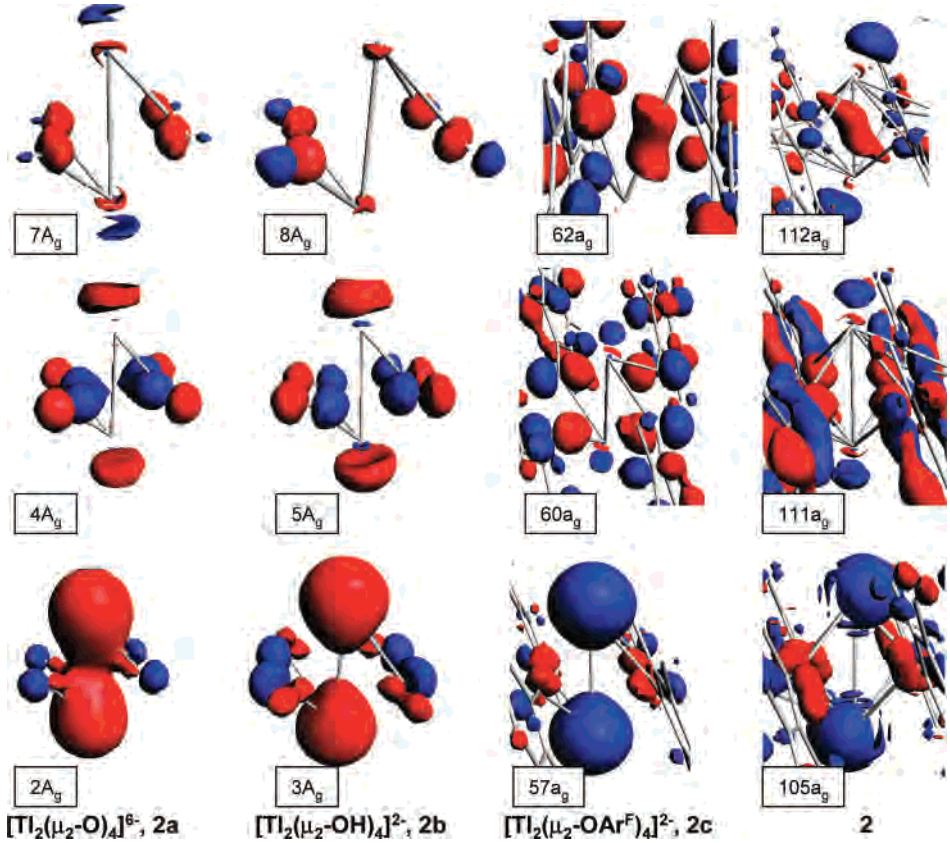

Figure 14. Comparison of orbitals in models **2a**, **2b**, and **2c** with compound **2**. Orbital representations for **2a** and **2b** are at the 0.05 $e^-/Å^3$ level and those for **2c** and **2** at the 0.03 $e^-/Å^3$ level.

Scheme 4

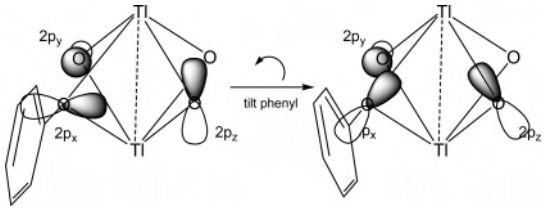

Tl···Tl vector in the b_u-type orbitals ($2b_u$, $6b_u$). Thus, only the a_g and b_u orbitals and not the a_u or b_g combinations overlap with the Tl 6s orbitals. The orbitals of a_g symmetry are most relevant to the Tl···Tl interaction.

In Figure 14, the a_g symmetry orbitals with significant thallium contributions from Figure 13 are compared with orbitals of similar symmetry and composition in the models **2b** and **2c** and compound **2**. The bonding picture changes little between **2a** and **2b** except for the participation of oxygen in O−H bonding in, for example, the orbital $3a_g$. With the introduction of the phenyl substituents, the reason for their slanted orientation becomes clear. Rotation of the C_6F_5 plane such that it is not parallel to the Tl···Tl vector facilitates greater overlap of the oxygen $2p_x$ and $2p_z$ with the Tl 6s orbitals, as shown in Scheme 4. The 2 p_y orbital is unaffected by the angle of the phenyl ring to the Tl···Tl vector. The model **2c** shows also that orbitals with thallium contributions also have large ligand contributions, making the Tl−O and Tl···Tl interactions harder to discern visually, but nonetheless present. Contour maps of the **2c** and **2** orbitals from Figure 14 are shown in Figure 15. The energies,

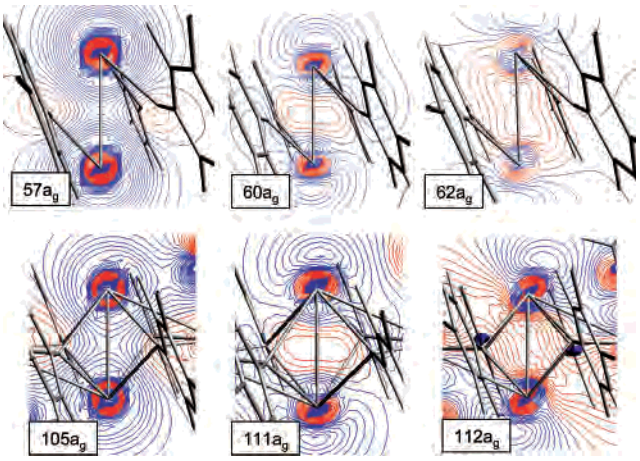

Figure 15. Contour maps of the orbitals with large Tl 6s contributions in model **2c** (top row, left to right) and **2** (bottom row, left to right). The 25 curves are spaced linearly between 10^{-1} and 10^{-5} $e^-/Å^3$.

occupancies, and fractional contributions to the a_g orbitals with significant Tl 6s contributions in **2c** and **2** are listed in Table 5. The molecular orbitals of **2c** show the same in-phase overlap as in **2a** and **2b** of Tl 6s orbitals with O $2p_x$ orbitals in $57a_g$ and a Tl−Tl nonbonding interaction in $60a_g$ (HOMO−3) due to the inward-pointing lobes of the O $2p_x$ orbitals. In $62a_g$ (LUMO+3), a Tl−Tl bonding combination with significant mixing of Tl 6s with Tl $5p_y$ orbital is observed.

The calculation of the complete **2** includes two additional thallium atoms and one THF molecule on each end that were absent in **2c**. The experimental distances (Å) and computa-

Table 5. Orbital Energies and Fractional Composition for Model **2c** and Compound **2**[a]

compound	MO	electrons	energy (eV)	Tl 6s	Tl $5p_x$	Tl $5p_y$	O $2p_x$	O $2p_z$
2c	$53a_g$	2	−5.2248	0.1209	−0.0064	0.0466	−0.1249	−0.1656
	$56a_g$	2	−3.6575	−0.393	−0.0256	0.0385	0.2943	−0.2221
	57a$_g$	***2***	***−2.9143***	***0.7709***	***−0.0042***	***−0.1123***	***0.1388***	***0.2199***
	$59a_g$	2	−1.5706	0.2001	0.1286	−0.0357	0.2609	−0.0877
	60a$_g$	***2***	***−0.69***	***0.237***	***−0.0624***	***−0.1424***	***0.6061***	***−0.0706***
	$61a_g$	0	2.9406	−0.1105	0.0265	0.053	0.0257	−0.1737
	62a$_g$	***0***	***3.1431***	***0.0591***	***−0.1512***	***−0.4406***	***0.1462***	***−0.061***
2	$88a_g$	2	−13.3012	−0.109	0.0171	−0.0058	0.0997	0.1748
	$90a_g$	2	−13.0485	−0.1485	−0.0087	−0.0127	0.0289	0.3371
	$91a_g$	2	−12.794	0.1242	0.0072	0.0275	−0.1055	−0.3149
	$95a_g$	2	−11.3553	0.1217	0.001	0.0129	−0.225	0.0521
	$96a_g$	2	−11.22	0.1545	−0.0067	0.0123	−0.2455	0.0445
	$98a_g$	2	−10.7786	0.101	0.017	0.0286	−0.2678	0.0604
	105a$_g$	***2***	***−8.9149***	***0.4609***	***0***	***−0.0024***	***−0.0727***	***0.177***
	$106a_g$	2	−8.1144	0.448	0.1131	−0.0273	−0.0378	0.1968
	$107a_g$	2	−7.8925	0.5851	−0.0696	−0.0685	0.1621	0.1854
	$108a_g$	2	−7.1859	−0.3226	−0.0793	0.0489	−0.3399	0.0543
	111a$_g$	***2***	***−5.8071***	***0.2719***	***−0.0399***	***−0.1543***	***0.5165***	***−0.0371***
	112a$_g$	***0***	***−1.8806***	***0.1779***	***−0.3412***	***−0.4575***	***0.0094***	***−0.0127***

[a] Entries corresponding to Figures 14 and 15 are shown in bold italics.

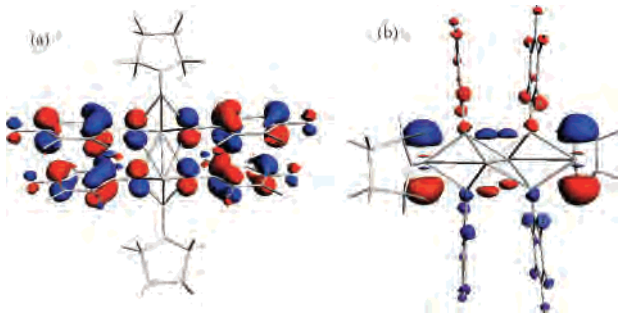

Figure 16. Molecular orbital representations (energies in eV) from DFT calculation of **2:** (a) HOMO b_g79 (−5.4174) and (b) LUMO a_u80 (−2.4935). All orbitals are shown at the 0.03 $e^-/Å^3$ level.

tional ones (in parentheses) agree well with one another including the distances Tl(1)..Tl(1) 3.5943(15) (3.460), Tl(1)···Tl(2) 3.9696(15) (3.977), Tl(1)−O(1) 2.656(4) (2.557), and Tl(1)−O(1_2) 2.844(4) (2.703). The HOMO ($79b_g$) of **2** is again a ligand-based π-type orbital (Figure 16a), but the LUMO ($80a_u$) (Figure 16b) is primarily localized on the THF-bound thallium Tl(2) (44%) and the solvent-free Tl(1) (36%). Shown in Figure 15 are three a_g symmetry orbitals with the same bonding patterns as in the three models. Orbital $105a_g$ shows an in-phase Tl···Tl overlap whose electron density is observed between the thallium nuclei (Figure 15). Figures 14 and 15 also show an occupied Tl···Tl nonbonding orbital ($111a_g$) and an unoccupied Tl−Tl bonding orbital ($112a_g$) that, like $80a_u$, may be populated in the exctited state (vide infra).

DFT calculations were also performed on the hypothetical dimers $(TlOAr')_2$, **I**, and $(TlOAr^F)_2$, **II**, on the basis of the atom positions from the X-ray diffraction structure of the $(TlOF^{mes})_2$ dimer (F^{mes} = 2,4,6-$OC_6H_2(CF_3)_3$).[58] The Tl_2O_2 rhombus is a common feature of Tl(I) coordination chemistry[37] and is present clearly in both **1** and **2**. It was postulated that the slight differences in ligand electronic structure might result in sufficient differences in electron densities on thallium and oxygen to account for different pairings of the Tl(2)O(2) rhombi in **1** and **2**. Mulliken charge analyses for **II** show charges of +0.6508 (Tl) and −0.7602 (O) whereas the related values for dimer **I** are +0.6282 (Tl) and −0.7640 (O). (Supporting Information, Figure S8) These differences are not significant enough to be the basis for the observed isomeric differences. This result suggests that the combination of thallophilic attraction and π-stacking facilitate the assembly of the $\{Tl_2(\mu_2\text{-}OAr^F)_4\}$ unit in **2**, in contrast to the cubane structure in **1**. The steric bulk of the meta CF_3 groups cannot prevent the assembly of such a $\{Tl_2(\mu_2\text{-}OAr)_4\}$ octahedron as shown by the structure of **5**.

Both compounds **1** and **2** show Stokes shifts in THF solution fluorescence spectra (Supporting Information, Figure S10) that reinforce the bonding picture of **1** and **2** from the X-ray diffraction and ^{203}Tl and ^{205}Tl NMR data. For **1**, with excitation at λ = 290 nm and emission at 315 nm, the shift is smaller than that of **2**, which for excitation at λ = 294 nm, has an emission at 347 nm. The greater shift in the spectrum of **2** to lower energy is consistent with emission from the lower-energy metal-based orbitals of the thallophilic interaction, such as $80a_u$ or $112a_g$ from the calculation of **2**. Another similar bridged thallophilic interaction has been reported recently.[80] Two thallium atoms are 3.7562(6) Å apart and bridged by two DMSO molecules and the gold atom of a $[Au(C_6F_5)_2]^-$ anion. As in the case of **2**, the close contact observed in the solid state is retained in solution, as demonstrated by room-temperature fluorescence.

Summary

Two different tetrameric isomers of thallium fluorinated aryloxides have been structurally characterized. A cubane is observed in $(TlOAr')_4$, and a new motif in thallium aryloxides, a pseudo-octahedral $\{Tl_2(\mu_2\text{-}OAr^F)_4\}$ unit is observed with the OAr^F ligand. The $\{Tl_2(\mu_2\text{-}OAr^F)_4\}$ moiety contains a thallophilic contact at 3.5943(15) Å whose existence is supported by fluorescence spectroscopy. The retention of the cluster units in solution has been demon-

(80) Fernandez, E. J.; Laguna, A.; Lopez-de-Luzuriaga, J. M.; Montiel, M.; Olmos, M. E.; Perez, J. *Inorg. Chim. Acta* **2005**, *358*, 4293−4300.

strated with VT ^{205}Tl and ^{203}Tl NMR spectroscopy. Spectral deconvolution shows that the cubane structure of $(TlOAr')_4$ is retained, and a more complicated coupling pattern in the case of $(TlOAr^F)_4$ suggests that a noncubane structure persists in this case. The structures of the heterobimetallic species $[Tl_2Cu(OAr^F)_4]$ and $[Tl_2Cu(OAr')_4]$ compounds also exhibit the $\{Tl_2(\mu_2\text{-}OAr^F)_4\}$ motif with Tl···Tl contacts of 3.86(6) (average over five) and 3.564(1) Å, respectively. The formation of the thallophilic interactions may be facilitated by π-stacking between the OC_6F_5 ligands, but it is not prevented by bulkier CF_3 groups on the aryloxide moieties because it is observed in complexes with both types of ligand. DFT calculations describe the orbital basis of this interaction with the $\{Tl_2(\mu_2\text{-}OAr^F)_4\}^{2-}$ unit.

Acknowledgment. This work was supported by start-up funds from Barnard College, a Camille and Henry Dreyfus Faculty Start-up Grant (SU-99-065), a Research Corporation CCSA Award (CC5398), PRF 38007-GB3 (to L.H.D.), and an NSF-CAREER award (to L.H.D.; CHE-0134817). We thank G. F. R. Parkin and D. G. Churchill for collecting the raw data for compound **3** and D. Bray, M. Wall, S. Kunz, and C. Miller for assistance with preliminary ^{205}Tl studies. T.M.A. (Sandia) was supported from the DOE BES program. Sandia is a multiprogram laboratory operated by Sandia Corporation, a Lockheed Martin Company, for the United States Department of Energy's National Nuclear Security Administration under Contract No. DE-AC04-94AL85000.

Supporting Information Available: Tl···F contacts in crystal structures; VT ^{205}Tl NMR spectra of **2** in acetone; DFT results; fluorescence spectra of **1** and **2**; and X-ray crystallographic data in CIF format. This material is available free of charge via the Internet at http://pubs.acs.org.

IC050955O